SUPPORTING INFORMATION

Shape-Dependent Relaxivity of Nanoparticle-Based T_1 Magnetic Resonance Imaging Contrast Agents

Kayla S.B. Culver,[a‡] Yu Jin Shin,[a‡] Matthew W. Rotz,[b] Thomas J. Meade,[b]* Mark C. Hersam,[a,b]* and Teri W. Odom[a,b]*

‡ These authors contributed equally

[a]Department of Materials Science and Engineering, and [b]Department of Chemistry, Northwestern University, Evanston, Illinois 60208, USA

* Corresponding authors:
tmeade@northwestern.edu, 847-491-2481
m-hersam@northwestern.edu, 847-491-2696
todom@northwestern.edu, 847-491-7674

Au nanostar synthesis and characterization

All reagents were purchased from Sigma-Aldrich (St. Louis, MO) unless otherwise noted. Au nanostars were synthesized by reduction of $HAuCl_4$ by (4-(2-hydroxyethyl)-1-piperazineethanesulfonic acid) (HEPES, Sigma-Aldrich product # 54457). Specifically, a stock of 1M HEPES buffer was prepared and pH was adjusted to 7.2 with NaOH. An aliquot of 40 mM $HAuCl_4$ was added to 100 mM HEPES (5 µl $HAuCl_4$ per 1 ml HEPES) and stirred for 1 minute, then the mixture was left undisturbed at room temperature for at least 30 minutes. Nanostars were stored in the growth solution at 4 °C. A Cary 5000 UV-vis-NIR spectrophotometer (Agilent Technologies, Santa Clara, CA) was used to characterize the optical properties of the nanoparticles from 400-1400 nm. Dynamic light scattering (DLS) was done with a ZetaPALS zeta potential and particle size analyzer (Brookhaven Instruments, Holtsville, NY). Photographs of the DGC tubes were taken with a Sony DSLR camera. Transmission electron microscopy (TEM) was used to characterize nanostar shapes and sizes. Particles were drop-cast onto TEM grids with carbon and formvar support films (Ted Pella, Inc., Redding, CA) and imaged on a JEOL 1230 TEM (Peabody, MA) using a 100 kV accelerating voltage. Au and Gd(III) quantification was performed by acid digestion of samples followed by inductively coupled plasma mass spectrometry (ICP-MS) analysis on a Thermo iCap Qc ICP-MS (Thermo Fisher Scientific, Waltham, MA, USA). ICP-MS samples were prepared as described previously.[1] Briefly, DNA-Gd@star samples were digested in 1:1 nitric acid:hydrocholoric acid (Nitric acid, >69% ; TraceSelect HCl, 37%). Milli-Q water and a multielement internal standard containing Bi, Ho, In, Li, Sc, Tb, and Y (Inorganic Ventures, Christiansburg, VA) were added to produce a solution of 2% nitric acid (v/v), 2% HCl (v/v), and 5.0 ng/mL internal standard up to a final

volume of either 3 or 10 ml. Serial dilutions of Gd and Au standards (Inorganic Ventures) were prepared in the same matrix as the samples.

Gd(III)-DNA synthesis and characterization

The Gd(III)-DNA is a poly deoxythymidine (dT) oligonucleotide (24-mer) that contains a 3' disulfide modification (for Au functionalization) and five covalently-bound Gd(III) chelates per strand. The Gd(III) chelate was synthesized according to previously reported protocols to contain a pendant alkyne group and had an optimized inner-sphere water exchange rate (τ_m=22 ns at 37 °C).[1] Coordination of this Gd(III) complex with only one inner sphere water molecule was previously determined (q=1.1 ± 0.1).[1] The reported r_1 (measured at 37°C, 1.41 T, 60 MHz) of the free Gd(III) complex and of the Gd(III)-DNA were 3.8 $mM^{-1}s^{-1}$ and 9.5 $mM^{-1}s^{-1}$, respectively.[1]

Synthesis of amine-modified oligonucleotide was performed on a MerMade automated synthesizer using standard phosphoramidite coupling chemistry and reagents purchased from Glen Research (Sterling, VA). Specifically, 3' disulfide C3 controlled pore glass beads were placed onto the synthesizer, with standard dT phosphoramidite and amino modifier C6 dT (Glen Research).[1] The synthesized oligonucleotide consisted of the sequence 3'–S-STTT-TTT-TTT-T*TT-T*TT-T*TT-T*TT-T*TT-Cy3–5' where positions bearing amine modified dT are indicated as T*, and a 5' Cy3 phosphoramidite was coupled manually after automated synthesis using similar coupling chemistry, but where CPGs were left to react overnight before purification (Glen Research). Trityl groups were removed from strands before deprotection from the resin by exposure to dicholoroacetic acid, followed by rinsing with acetonitrile and drying open to air. Subsequently, deprotection of the oligonucleotide from the solid phase was performed using standard 1:1 AMA conditions (ammonium hydroxide:methylamine) at 55 °C for one hour. Supernatant oligonucleotides were filtered away from CPGs, purified by reverse phase HPLC,

and characterized using MS-MALDI. Amine modified strands were dried by lyophilization (m/z) observed: 8763.9, calculated: 8761.7 $[M - H]^-$.

Incorporation of azide functionality was performed using 1 μmol of deprotected 5x amino modifier poly-dT DNA in 500 μL of pH 8.5 carbonate buffer (100 mM). Using 5 mg of azidobutyrate NHS ester (Glen Research) in 100 μL of DMSO, these solutions were mixed and the reaction was left to stir overnight. Complete reaction was confirmed by the loss of starting DNA by MALDI-MS. Azide DNA was purified by reverse phase HPLC, and dried by lyophilization (m/z) observed: 9331, calculated: 9327.31 $[M - H]^-$.

Attachment of Gd(III) to DNA begins with dissolution of 1 μmol of 5x azide bearing DNA into 500 μL of 1.5 M triethylammonium acetate buffer pH 7. To the mixture (via stock solutions, adapted from ref.[2]) is added 100 nmol Cu(II) sulfate, 500 nmol tris-hydroxypropyl triazolyl amine, 10 μmol of 5, and 1 μmol sodium ascorbate. The reaction is capped and allowed to stir overnight. The resulting 5x Gd(III)-DNA complex is then purified by reverse phase HPLC, characterized by MS-MALDI, and lyophilized (m/z) observed: 12373, calculated: 12372.31 $[M - H]^-$.

Surface functionalization with thiolated Gd(III)-DNA

Nanostars were functionalized with DNA by salt aging similar to reported procedures.[3] Specifically, 4.1 OD (260 nm) of protected, 3' thiolated DNA (corresponding to ~1500 strands of DNA per nanostar) was dried into a 1.5 mL microcentrifuge tube, to which is added 300 μL of 100 mM dithiothreitol in 180 mM (pH 8.0) phosphate buffer. The solution was stirred at room temperature for 1 hour and the DNA was run through a pre-packed G25 sephadex column (NAP-5, GE Life Sciences) using 180 mM phosphate buffer as the eluent, and observing the Cy3 dye visually to monitor elution. After purification of deprotected DNA, the eluent solution was used directly for functionalization of unsorted (post-sucrose exposed) nanostars, or divided into fractional aliquots corresponding to the relative concentrations of sorted nanostar fractions.

For example, to an unsorted batch of nanostars (6 mL at 2.1 nM) was added 6.4 μL of Tween 20 (0.01% v/v) and deprotected and purified DNA (4.7 OD_{260}) in 0.3 mL of 180 mM phosphate buffer pH 8.0. The solution was sonicated for 30 seconds and left to stir for 30 minutes. Over the next five hours, an aqueous stock of NaCl (4.753 M), phosphate buffer (10 mM) and 0.01% Tween 20 were added in increments of 155, 159, 163, 167 and 171 μL per hour, with each addition followed by 30 seconds of sonication. During the intervening time, the solution is left to stir at room temperature. The final concentration of NaCl is 612.5 mM. Salted particles were then left to stir for a further 48 hours. Likewise, each fraction of sorted stars was individually functionalized.

After functionalization, DNA-Gd@stars were purified 3x by centrifuging (10,000 RPM, 10 min), removing the supernatant, sonicating the pellet, then resuspending in Milli-Q water with 0.01% Tween. As a comparison, 80-nm spherical Au colloids (Ted Pella, Inc.) were

functionalized with Gd(III)-DNA using the same procedure using a concentration of DNA corresponding to 10,000 DNA/particle.

Density gradient centrifugation

Density gradient centrifugation (DGC) is a type of post-synthetic separation technique that exploits differences in centrifugal sedimentation rates of materials through a viscous density gradient.[4] DGC conditions were optimized to achieve nanostar band spreading throughout the centrifugation tube. Sucrose density gradients were formed using a linear density gradient maker (SG Linear Density Gradient Maker, Hoefer, Inc., Holliston, MA) with 9 ml starting solutions of 50% and 60% w/v (density: 1.42-1.45 g/cm^3) on top of a 4 mL underlayer of 90% w/v sucrose in water. A concentrated solution of bare Au nanostars (8-10 nM) was loaded on top of the density gradient medium in an Ultra-Clear centrifuge tube (Beckman Coulter, Brea, CA), then centrifuged at 4400 x *g* for 2 hours at 22 °C using a Beckman SW32Ti rotor in a Beckman Optima L-80XP ultracentrifuge. The samples were fractionated at intervals of 2 mm from the meniscus (Biocomp Instruments, Fredericton, NB, Canada). This process was repeated 26 times, and the corresponding fractions (i.e. same sedimentation distance) from the 26 sorted tubes were combined to obtain sufficient concentrations for relaxivity measurements (typically 200-400 µl of 5-8 nM nanostars per fraction). After combining the fractions, the samples were and dialyzed (20,000 MWCO, Thermo Scientific) overnight against ultra pure deionized water to remove excess gradient media. To minimize variables when comparing sorted and unsorted DNA-Gd@stars, nanostars were exposed to sucrose for 2 h without sorting prior to functionalization to use as the unsorted control (post-sucrose functionalized).

Stability testing of nanostars in gradient media

Anisotropic Au NPs without strongly-bound stabilizing surfactants (e.g. CTAB and CTAC) have not yet been sorted with DGC. Thus, we determined the gradient media type and exposure conditions that were compatible with the shape, colloidal stability, and DNA-functionalization of Au nanostars. The most common media used as the density gradient to sort Au NPs are iodixanol (Optiprep) and sucrose because they are non-ionic and form stable gradients.[4-8] We imitated the conditions that were used for DGC of nanostars with both media, but without the centrifugation and fractionation (separation) steps in order to isolate the effects of the gradient media and to compare particles with the same distribution of shape populations. TEM, UV-vis, DLS, DNA-loading, and relaxivity were analyzed for particles under each condition. *As-functionalized* DNA-Gd@stars were prepared by functionalizing nanostars with Gd(III)-DNA and purifying as described above (no exposure to gradient media). For *pre-sucrose* and *pre-iodixanol functionalized* conditions, these DNA-Gd@stars (8-10 nM) were then mixed into solutions of sucrose (55% w/v) or iodixanol (30% w/v) and exposed for 2 h. Then the solutions were dialyzed overnight in ultra pure deionized water to remove the excess gradient media. Particles were recovered and concentrated via centrifugation prior to analysis. For *post-sucrose* and *post-iodixanol functionalized* particles, bare nanostars (8-10 nM) were first exposed to the gradient media and dialyzed under the same conditions. Then, the sucrose-exposed and iodixanol-exposed nanostars were functionalized with Gd(III)-DNA and purified for analysis.

Branch number, size, and DNA loading analysis

Structural characterization was based on analysis of TEM images of DNA-Gd@stars (Fig. S1) which were taken from several areas on the grid to obtain representative populations. The branch number was manually counted on at least 400 particles in each fraction. Due to the 3D structure of nanostars, it is possible for some branches to be obscured in the 2D projection (e.g. some particles counted as 7 branches may have had one hidden branch that could not be counted). However, the nanostars typically fall at angles with the branches not perfectly overlapping so they can be identified. Thus, we believe the manual counting resulted in accurate or slightly underestimated branch numbers. The "analyze particles" plugin of ImageJ was used to automatically measure parameters such as "Feret diameter" and "fit ellipse" for at least 275 particles in each fraction. The maximum Feret diameter typically corresponds to the longest tip-to-tip dimension of the nanostar (Table S1). The average particle volume was estimated for unsorted and sorted fractions of DNA-Gd@stars based on the best fit ellipse and assumptions about the out-of-plane dimensions. This method allows for high throughput estimations from many particles. The fit ellipse function provides the dimensions of an ellipse *with the same area* and orientation of each nanostar projection. We assumed that the out-of-plane dimension of a particle could be approximated by the average of the major and minor axes of the fit ellipse. The volume of each nanostar was then calculated as an ellipsoid. Particle mass was calculated from the volumes and the density of bulk Au (19.30 g/cm^3). The number of Au atoms per particle was calculated based on the volume and the density and molecular weight (196.97g/mol) of bulk Au (59.1 atoms per nm^3). Gd(III)-DNA loading per particle was determined by ICP-MS analysis of the Gd(III) and Au content of purified DNA-Gd@stars. Each strand of Gd(III)-DNA contains

five Gd(III) chelates,[1] and the number of Au atoms per nanostar determined the particle concentration.

r_1 (relaxivity) measurement

After Gd(III)-DNA functionalization of each sored fraction and unsorted control, the r_1 relaxivity was calculated by measuring the T_1 relaxation times and Gd(III) concentrations at a clinically relevant temperature (37 °C) and field strength (1.41 T, 60 MHz). Specifically, a stock of each DNA-Gd@stars sample was diluted serially (3-5 dilutions) into water (0.01% Tween20). Using a 150 uL aliquot of each dilution, T_1 relaxation times were measured using a Bruker MiniSpec60 (Billerica, MA) at 37 °C and 1.41 T (60 MHz) as a function of Gd(III) concentration. ICP-MS metal analysis was used for determination of the Gd(III) concentration and these data were plotted as $1/T_1$ versus [Gd(III)] (mM) followed by linear regression analysis. The resulting fit of the line is defined as the r_1 relaxivity of the agent (Fig. S6-S8). For the sorted fractions, measurements were repeated on each sample.

Characteristics of unsorted and sorted DNA-Gd@stars

Table S1 summarizes the average structural features (Feret diameter, estimated mass, % of many- and few-branched particles, and the ratio of many- to few- branched particles) and relaxivity of unsorted and sorted DNA-Gd@stars The Feret diameter and estimated mass of the DNA-Gd@stars increased rapidly at first with increasing fraction number, but remained similar between fractions #20-28. The percentage of many-branched particles peaked at fractions #22-24 then began to decrease in higher fraction numbers (farther sedimentation distance). Similarly, the percentage of few-branched particles was minimized in fractions #22-24 then began to increase in higher fraction numbers. Fractions near the top of the gradient (#6-12) contained the highest percentage of few-branched particles and the lowest percentage of many-branched particles. The ratio of many- to few- branched DNA-Gd@stars is a parameter that allows for consideration of the contributions of both types of populations and was highest in fraction #22. The highest relaxivity occurred in fraction #22 (57.3 $mM^{-1}s^{-1}$). This relaxivity is 15-fold larger than that of the alkyne-bearing Gd(III) chelate (prior to binding to the DNA) and 6-fold larger than that of the Gd(III)-DNA (prior to functionalization on the NPs) used in this study. The lowest relaxivity of DNA-Gd@stars occurred in fraction #6, though was still higher than that of DNA-Gd@spheres of various sizes.

Fraction	Feret diameter (nm)	σ (nm)	Estimated mass (fg)	σ (fg)	% of many-branched	% of few-branched	Ratio of many:few branched	r_1 (mM^{-1} s^{-1})	σ (mM^{-1} s^{-1})
Unsorted	61	19	0.7	0.4	31.0	27.4	1.13	45.2	3.0
6	35	9	0.14	0.07	6.4	40.3	0.16	27.9	0.6
11	53	14	0.4	0.2	12.6	45.7	0.27	36.3	1.9
12	55	15	0.5	0.2	8.8	47.6	0.18	34.8	0.9
16	65	18	0.8	0.3	24.9	33.0	0.76	35.6	1.4
20	74	19	1.1	0.5	50.2	13.3	3.78	56.4	1.1
22	76	18	1.2	0.5	58.1	9.4	6.17	57.3	1.4
24	74	20	1.2	0.6	58.7	13.0	4.53	56.1	4.0
27	78	19	1.3	0.5	53.7	17.2	3.13	48.2	1.7
28	74	21	1.3	0.8	48.4	21.0	2.31	40.9	2.3
Sphere	15[a]		0.03		N/A		N/A	14.6[a]	
	40[a]		0.65					16.9[a]	
	80		5.18					25.2	

Table S1. Summary of structural features and relaxivity of the unsorted and sorted DNA-Gd@stars, and DNA-Gd@spheres of different sizes. σ = standard deviation of the mean. [a] Data from ref.1.

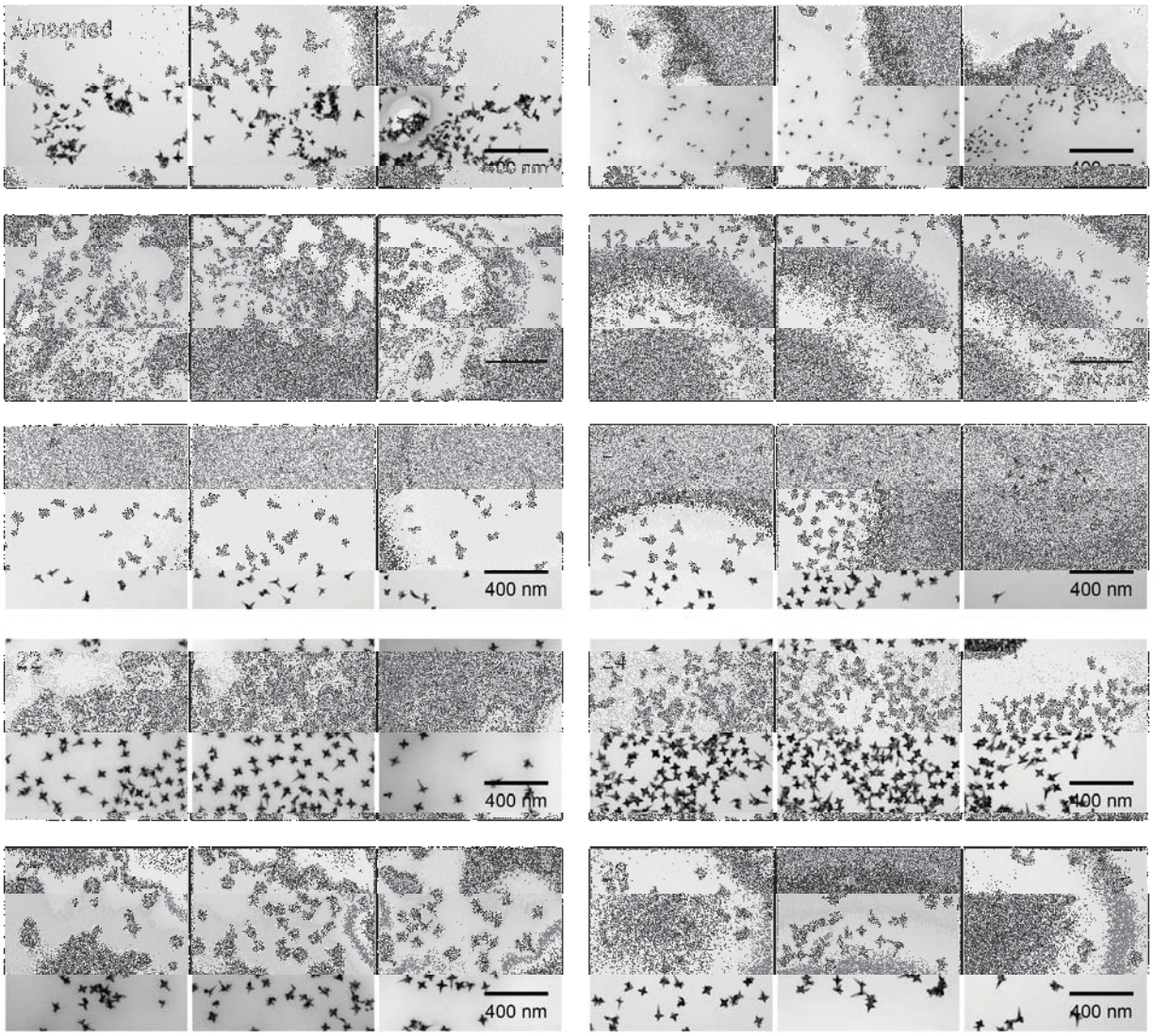

Figure S1. Examples of zoomed-out TEM images used for structural analysis. Unsorted and each sorted fraction of DNA-Gd@stars. Approximately 10 such images, taken from various locations on the TEM grid, were used for branch counting and size analysis.

Figure S2a shows the extinction spectra of unsorted and sorted DNA-Gd@stars. The largest LSP peak of DNA-Gd@stars red-shifted with increasing fraction number (Fig. S2b, black), but began to level off through fractions #22-28. This corresponds well with the observed leveling off of size and branch numbers. Additionally, the full width at half maximum (FWHM) of the main resonance peak decreased, by up to 14%, from the unsorted sample to fraction #22, and then increased through fraction #28 (Fig. S2b, red). This resonance narrowing corresponds with the increased homogeneity of the particle shapes and sizes. The FWHM of fractions 6-12 is not shown because multiple peaks are convoluted.

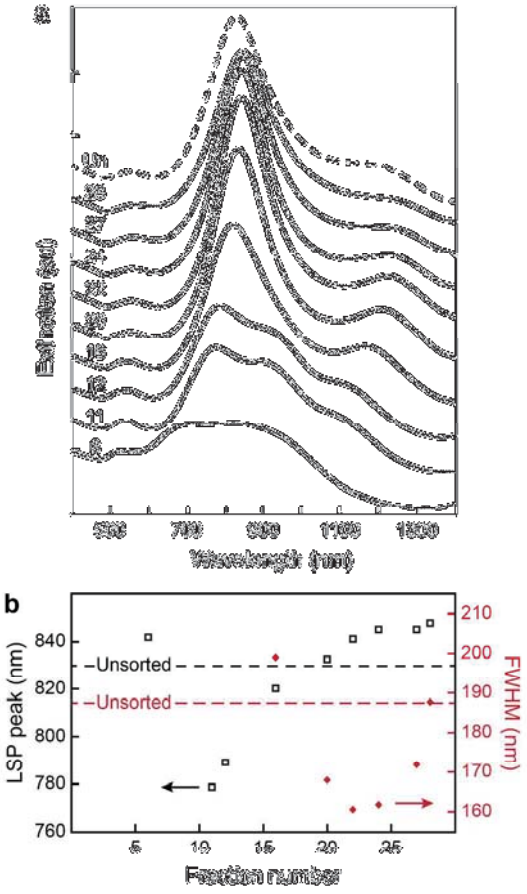

Figure S2. Optical properties of unsorted and sorted DNA-Gd@stars. (**a**) Normalized extinction of sorted and unsorted DNA-Gd@stars. (**b**) A red-shift in the primary LSP peak position (black) is observed with increasing fraction number. The FWHM (red) is narrowest in fraction 22. Dashed lines: unsorted (post-sucrose functionalized).

Stability testing of nanostars in gradient media

We found that the branched shape (Fig. S3, Fig. 1b-c), optical properties, and colloidal stability (Fig. S4) of nanostars and DNA-Gd@stars were not affected by sucrose using either pre- or post-sucrose functionalization methods compared to as-functionalized DNA-Gd@stars. However, there was a difference in the DNA-loading between the three samples (Fig. S5a). Pre-sucrose functionalization resulted in a slight decrease in DNA loading per particle compared to the as-functionalized DNA-Gd@stars, which we attribute primarily to DNA loss during dialysis. Interestingly, the DNA loading on post-sucrose functionalized particles was almost double that of the as-functionalized DNA-Gd@stars. Since the pH during functionalization can affect DNA loading onto Au NPs,[9] we hypothesize that the increased DNA loading may be attributable to a reduction in pH of the nanostar solution after dialysis. Relaxivity was measured at the clinically relevant field strength of 1.41 T (60 MHz) at 37 °C. Although a slight difference in r_1 of the DNA-Gd@stars was observed under each condition (Fig. S5b-S6), all were within the range previously reported for DNA-Gd@stars[1] and are among the highest reported for NP-[10] or protein-bound[11-13] contrast agents with a Gd(III) chelate containing only one coordinated water molecule. These results indicate that sucrose is compatible with surfactant-free anisotropic NPs and biomolecule surface functionalization. Additionally, post-sucrose functionalization conditions are preferable due to increased DNA loading and for practical considerations (reduced amount of ligand are required to functionalize NPs after DGC compared to pre-sucrose functionalization).

Conversely, after exposure to iodixanol, pre-iodixanol functionalized DNA-Gd@stars reshaped to spheres (Fig. 1c), while iodixanol-exposed nanostars (Fig. S3c) and post-iodixanol functionalized DNA-Gd@stars (Fig. 1b) also contained a mixture of rounded particles with a few

blunt protrusions. The Au nanostars and DNA-Gd@stars (pre- and post- iodixanol functionalized) showed a blue shift in the LSP peak and a decrease in the hydrodynamic diameter (Fig. S4), which resulted from particle reshaping. Both pre- and post-iodixanol functionalized DNA-Gd@stars also showed dramatically reduced DNA loading per-particle and relaxivity per-Gd(III) (Fig. S5-S6). We expect the reduced DNA loading is due to decreased surface area, and the lower relaxivity is due to loss of the branched nanostar structure, both a result of the reshaping. These results indicate that iodixanol is not compatible with some types of surfactant-free anisotropic Au NPs and that gradient media compatibility should be characterized for DGC of functionalized Au nanoconjugates.

Iodixanol has previously been used to sort spherical Au NPs [7, 14-15] or anisotropic Au NPs that are coated in strongly-bound surfactants CTAB[5] or CTAC[6], but no changes in shape have been reported. Spherical Au NPs are unlikely to change shape because their shape is more thermodynamically stable than anisotropic NPs. Although CTAB and CTAC have been effective at maintaining the structure of anisotropic Au NPs in the presence of iodixanol, we hypothesize that the surface of Au nanostars, which is stabilized by HEPES molecules or thiolated DNA, is susceptible to reshaping via interaction with iodixanol. Other studies have found that changing the molecules that interact with the nanostar surfaces (e.g. introducing CTAB to PVP-stabilized nanostars) can result in reshaping to spheres via an Ostwald ripening process.[16]

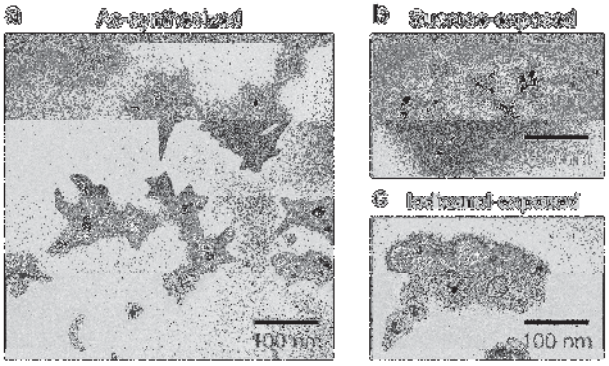

Figure S3. Structural stability of as-synthesized and sucrose- or iodixanol-exposed nanostars. TEM of **(a)** as-synthesized, **(b)** sucrose-exposed, and **(c)** iodixanol-exposed nanostars.

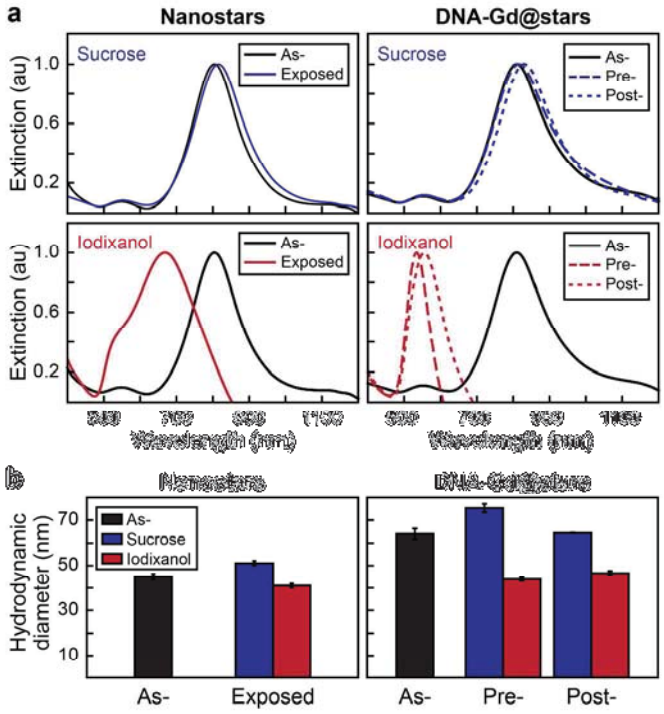

Figure S4. Optical and colloidal stability of nanostars and DNA-Gd@stars after exposure to sucrose or iodixanol. (a) Extinction spectra of sucrose- or iodixanol- exposed nanostars and DNA-Gd@stars compared to as-synthesized and as-functionalized. **(b)** Hydrodynamic diameter of nanostars and DNA-Gd@stars suggests that exposure to sucrose or iodixanol does not cause aggregation, but iodixanol causes a decrease in hydrodynamic diameter, which is consistent with the particles reshaping.

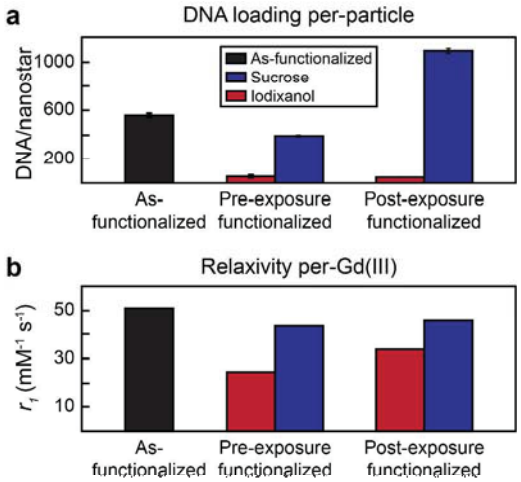

Figure S5. Gradient media compatibility with surface functionalization and relaxivity of DNA-Gd@stars. Effects of sucrose and iodixanol exposure on the **(a)** DNA loading per-particle, and **(b)** relaxivity per-Gd(III) of DNA-Gd@stars.

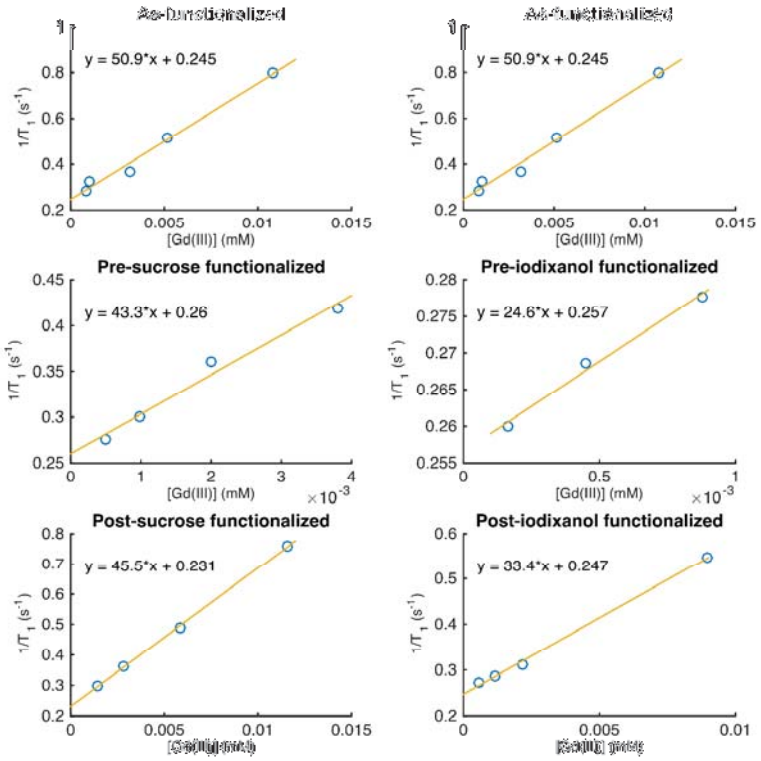

Figure S6. Relaxivity calculations for DNA-Gd@star stability tests in sucrose (left) and iodixanol (right).

Relationship between shape and relaxivity

The r_1 of a Gd(III)-based contrast agent measures enhancements in the longitudinal (T_1) relaxation rate of water normalized to the concentration of Gd(III) (Fig. S7). An increase in r_1 corresponds to increased brightness in T_1 weighted MRI images, thus a reduction in the Gd(III) concentrations required to observe this contrast. It is important to note that for NP-based contrast agents, per-Gd(III) r_1 is not simply a function of the amount of Gd(III) loading per NP: changes in per-Gd(III) r_1 are due to altering the relaxation efficiency of each Gd(III) chelate. Typical methods to alter the r_1 of Gd(III) agents include changing the rotational correlation time, the inner-sphere water exchange rate, or the number of coordinated water molecules.[1, 11] In the case of previously reported DNA-Gd@stars, however, nuclear magnetic relaxation dispersion (NMRD) analysis showed that the exceptionally high r_1 was due to a large contribution of second-sphere relaxivity, related to slowed water diffusion near the Gd(III) chelates.[1] This effect was not observed on the DNA-Gd@spheres, thus we hypothesized that the nanostar shape, specifically regions of negative curvature between branches, could lead to DNA crowding and the altered water diffusion.[1] Here, we have investigated in more detail how the populations of branch numbers contribute to these relaxivity enhancements within in a batch of DNA-Gd@stars.

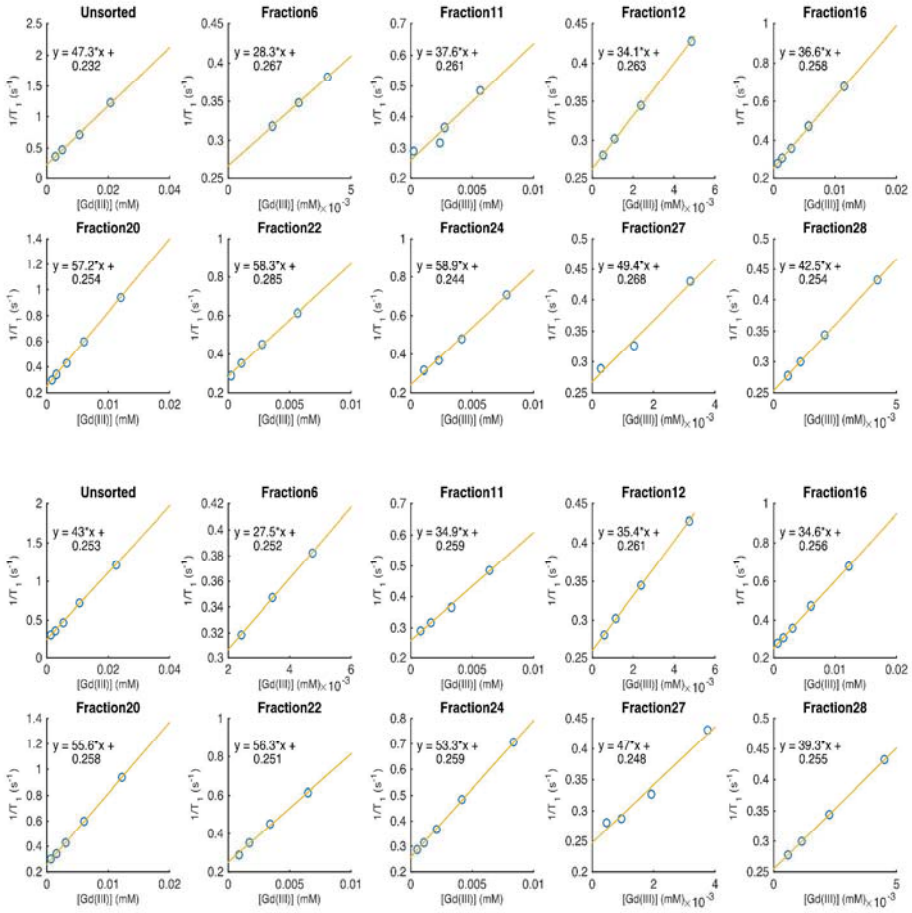

Figure S7. Relaxivity calculations for unsorted and sorted DNA-Gd@stars. Two measurements (top and bottom) were performed on each sample.

Relationship between size and relaxivity

Average Feret diameters and mass (Table S1), as determined by ImageJ analysis of TEM images, indicate that Au nanostar size generally increases with increasing fraction number (increasing sedimentation distance). In particular, average nanostar Feret diameter, mass, and volume showed a rapid increase from the top to the middle part of the centrifuge tube (#6-20), and then began to level off between fractions #22-28. There was no significant difference between the average volumes from fractions #22-28 ($p>0.15$, ANOVA). Although there is a difference in the size of the nanostars in each population, our data (Table S1) and previous analysis[1] strongly suggests that size is not the major contributing factor for the differences in r_1. In addition to comparing to our previously reported 15- and 40- nm spherical DNA-Gd@spheres, we functionalized 80-nm Au spheres with Gd(III)-DNA (Fig. S8), which are comparable in diameter to the largest fractions of DNA-Gd@stars, but have a volume (and mass) almost 4x larger than the largest nanostars (Table S1). In contrast to the surface of nanostars, spherical Au NPs have relatively uniform positive surface curvature. Fraction #6 showed the smallest average Feret diameter (35 nm) and a relaxivity of 27.9 $mM^{-1}s^{-1}$, which is almost 70% higher than 40- nm DNA-Gd@spheres (16.9 $mM^{-1}s^{-1}$),[1] and still slightly higher than that of 80-nm DNA-Gd@spheres (25.2 $mM^{-1}s^{-1}$). This comparison suggests that even few-branched nanostars are able to enhance the relaxivity of surface-bound Gd(III) compared to spheres over a wide size range. Furthermore, according to our previously reported nuclear magnetic relaxation dispersion (NMRD) analysis,[1] the rotational correlation time (the molecular parameter related to conjugate size and rotational diffusion) for both DNA-Gd@stars and 15-nm DNA-Gd@spheres was assumed to be sufficiently large to have minimal effects on the fitting. In other words,

consideration of size effects alone was not sufficient to explain the exceptionally high r_1 observed on DNA-Gd@stars.

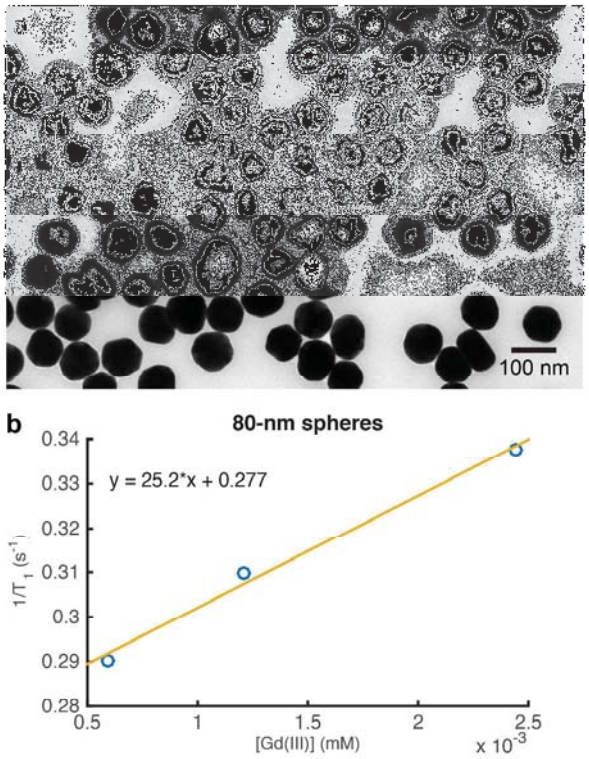

Figure S8. (a) Zoomed-out TEM and **(b)** relaxivity calculations for 80-nm DNA-Gd@spheres support the claim that size is not the primary factor for the relaxivity enhancements seen on DNA-Gd@stars.

Supplemental References

(1) Rotz, M. W.; Culver, K. S. B.; Parigi, G.; MacRenaris, K. W.; Luchinat, C.; Odom, T. W.; Meade, T. J. High Relaxivity Gd(III)–DNA Gold Nanostars: Investigation of Shape Effects on Proton Relaxation. *ACS Nano* **2015,** *9*, 3385-3396.

(2) Hong, V.; Presolski, S. I.; Ma, C.; Finn, M. G. Analysis and Optimization of Copper-Catalyzed Azide–Alkyne Cycloaddition for Bioconjugation. *Angew. Chem., Int. Ed.* **2009,** *48*, 9879-9883.

(3) Hurst, S. J.; Lytton-Jean, A. K. R.; Mirkin, C. A. Maximizing DNA Loading on a Range of Gold Nanoparticle Sizes. *Anal. Chem.* **2006,** *78*, 8313-8318.

(4) Xiong, B.; Cheng, J.; Qiao, Y.; Zhou, R.; He, Y.; Yeung, E. S. Separation of Nanorods by Density Gradient Centrifugation. *J. Chromatogr. A* **2011,** *1218*, 3823-3829.

(5) Tyler, T. P.; Lin, P. A.; Tian, Y.; Gao, H.-J.; Gao, X. P. A.; Sankaran, R. M.; Hersam, M. C. Centrifugal Shape Sorting of Faceted Gold Nanoparticles Using an Atomic Plane-Selective Surfactant. *J. Phys. Chem. Lett.* **2012,** *3*, 1484-1487.

(6) Shin, Y. J.; Ringe, E.; Personick, M. L.; Cardinal, M. F.; Mirkin, C. A.; Marks, L. D.; Van Duyne, R. P.; Hersam, M. C. Centrifugal Shape Sorting and Optical Response of Polyhedral Gold Nanoparticles. *Adv. Mater.* **2013,** *25*, 4023-4027.

(7) Tyler, T. P.; Henry, A.-I.; Van Duyne, R. P.; Hersam, M. C. Improved Monodispersity of Plasmonic Nanoantennas via Centrifugal Processing. *J. Phys. Chem. Lett.* **2011,** *2*, 218-222.

(8) Fruhnert, M.; Kretschmer, F.; Geiss, R.; Perevyazko, I.; Cialla-May, D.; Steinert, M.; Janunts, N.; Sivun, D.; Hoeppener, S.; Hager, M. D., et al. Synthesis, Separation, and Hypermethod Characterization of Gold Nanoparticle Dimers Connected by a Rigid Rod Linker. *J. Phys. Chem. C* **2015,** *119*, 17809-17817.

(9) Dam, D. H. M.; Lee, H.; Lee, R. C.; Kim, K. H.; Kelleher, N. L.; Odom, T. W. Tunable Loading of Oligonucleotides with Secondary Structure on Gold Nanoparticles through a pH-Driven Method. *Bioconjugate Chem.* **2015,** *26*, 279-285.

(10) Courant, T.; Roullin, V. G.; Cadiou, C.; Callewaert, M.; Andry, M. C.; Portefaix, C.; Hoeffel, C.; de Goltstein, M. C.; Port, M.; Laurent, S., et al. Hydrogels Incorporating GdDOTA: Towards Highly Efficient Dual T1/T2 MRI Contrast Agents. *Angew. Chem., Int. Ed.* **2012,** *51*, 9119-9122.

(11) Caravan, P.; Parigi, G.; Chasse, J. M.; Cloutier, N. J.; Ellison, J. J.; Lauffer, R. B.; Luchinat, C.; McDermid, S. A.; Spiller, M.; McMurry, T. J. Albumin Binding, Relaxivity, and Water Exchange Kinetics of the Diastereoisomers of MS-325, a Gadolinium(III)-Based Magnetic Resonance Angiography Contrast Agent. *Inorg. Chem.* **2007,** *46*, 6632-6639.

(12) Min, J.; Jung, H.; Shin, H.-H.; Cho, G.; Cho, H.; Kang, S. Implementation of P22 Viral Capsids as Intravascular Magnetic Resonance T1 Contrast Conjugates via Site-Selective Attachment of Gd(III)-Chelating Agents. *Biomacromolecules* **2013,** *14*, 2332-2339.

(13) Aime, S.; Delli Castelli, D.; Terreno, E. Novel pH-Reporter MRI Contrast Agents. *Angew. Chem., Int. Ed.* **2002,** *41*, 4334-4336.

(14) Sun, X.; Tabakman, S. M.; Seo, W.-S.; Zhang, L.; Zhang, G.; Sherlock, S.; Bai, L.; Dai, H. Separation of Nanoparticles in a Density Gradient: FeCo@C and Gold Nanocrystals. *Angew. Chem., Int. Ed.* **2009,** *48*, 939-942.

(15) Ko, S. H.; Vargas-Lara, F.; Patrone, P. N.; Stavis, S. M.; Starr, F. W.; Douglas, J. F.; Liddle, J. A. High-Speed, High-Purity Separation of Gold Nanoparticle-DNA Origami Constructs Using Centrifugation. *Soft Matter* **2014,** *10*, 7370-7378.
(16) Rodriguez-Lorenzo, L.; Romo-Herrera, J. M.; Perez-Juste, J.; Alvarez-Puebla, R. A.; Liz-Marzan, L. M. Reshaping and LSPR Tuning of Au Nanostars in the Presence of CTAB. *J. Mater. Chem.* **2011,** *21*, 11544-11549.